Scopolamine Alkaloid as Novel Green Inhibitor of Malleable Fe Corrosion Studied by EIS, DFT, PDP and SEM Techniques

B. U. Ugi[1]*, J. E. Boekom[2], P. B. Ashishie[1] and P. U. Ubua[1]

[1]*Department of Pure and Applied Chemistry, University of Calabar, Calabar, Nigeria*
[2]*Department of Chemistry, University of Uyo, Uyo, Nigeria*
*Corresponding author: ugibenedict@gmail.com

Received 01/05/2023; accepted 25/09/2023
https://doi.org/10.4152/pea.2025430103

Abstract
SAA as novel green inhibitor of MFe corrosion studied by EIS, DFT, PDP and SEM was investigated. It was observed that the increase in SAA various Ct triggered the rise in corrosion IE(%) up to 90.6, 97.6, 98.3 and 98.7%, as shown by EIS, PDP, WL and geometric techniques, respectively. This was due to high R_{ct} during electrochemical processes, which reduced $I_{corr,}$ and to SAA molecules strong adsorption onto the MFe surface. DFT results revealed short ΔE between SAA and MFe bands, which gave rise to faster inhibitor molecular transfer, stronger adsorption and increased inhibition. Thermodynamic assessment showed that SAA caused an exothermic reaction, creating a stable and spontaneous adsorption reaction. A physical adsorption mechanism was proposed from Langmuir's isotherm results.

Keywords: alkaloids; corrosion; electrochemistry studies; inhibition; quantum chemical calculations; SAA.

Introduction•

Metals are widely used in today's world, especially in the fields of engineering, such as shipping, building, construction, machining, automobile, petroleum, and mining [1-3]. Although the attractiveness and strength experienced from this metals while in use allow for their wider application, they are deeply affected by corrosion damage. Corrosion hinders metals' durability, tensile strength, malleability, ductility, conductivity, lustrous, etc. Being the deterioration of a metal under unfavorable surrounding conditions [2, 4], corrosion seems difficult to manage, considering the different growing environmental conditions experienced today, especially from green house effects. Corrosion causes are widely attributed to electrochemical or chemical processes involved in the preparation and treatment of metals before their application, such as acid pickling, acidification, descaling and fracking processes. [1, 3-5].

• The abbreviations and symbols definition lists are in pages 31-32.

Chemical CI have posed serious threat to the environment and the ecological system, since they are expensive to produce, difficult to procure (not easily assessable), and dangerous to health [1-5].
Therefore, since efforts have been taken in establishing alternative means to combat corrosive effects, plant extracts are mostly in use today in the area of corrosion mitigation [2, 3, 5-7]. These group of CI are desirable, since they are ecologically friendly, inexpensive to produce, easily assessable and harmless to living beings [2, 4, 8]. The interesting thing about plants is that they also possess hetero atoms (P, S and N), which are found in the presence of the hetero compounds (s), characteristics that portray them as good inhibitors [9, 10].
MFe is made by continuous heating and cooling of white Fe. This process allows for the release of graphite molecules into the Fe carbide. Products made from this MFe bend without breaking, and offer a decent tensile strength. MFe is used in fences, pipes and electrical fittings, washers, tools, farm equipment and implements and machine parts [10-12]. SAA is a major alkaloid of *Cnidoscolus aconitifolius* plant, which is popularly named as tree spinach. Its leaves are very high in protein, Ca, Fe, carotene and A, B and C vitamins.
The research target of this study was New Jerusalem Community in Obudu, Nigeria, where there are severe corrosion effects on tools/farm equipment and implements produced from MFe. It is believed that this research may promote the utilization of major alkaloids on these plants, for solving these corrosion effects.

Experimentation

Electrochemical experiment

A Gamry Reference 600 potentiostat was used. MFe, SCE and a 1 cm^2 Pt foil were used as working, reference and counter electrodes, respectively. Electrochemical tests were conducted. With R_{ct} and I_{corr} data, EI(%) obtained from EIS and PDP were calculated using Eqs. 1 and 2, respectively.

$$\% A = \frac{r_{ct}^0 - r_{ct}^i}{r_{ct}^0} x\ 100 \quad (1)$$

$$\% J = 100\left[1 - \frac{I_{corr}^i}{I_{corr}^0}\right] \quad (2)$$

where r_{ct}^0 and r_{ct}^i and I_{corr}^0 and I_{corr}^i represent R_{ct} and I_{corr} in HCl without and with SAA, respectively.

Computational method

This was carried out using Material Studio (version 8.0) software. Theoretical information, including E_{HOMO}, E_{LUMO}, ΔE, π, η and σ, was derived according to [13, 14].

WL experiment

Soxhlet extraction method was adopted for the crude SAA extraction, while a separating funnel was used for the alkaloid extraction, according to previous works of [15-17]. 5 g were used to make the stock solution from where serial dilution into different Ct of 1.0, 2.0, 3.5, 5.0 and 7.5 g/L were prepared. 100 mL

beakers containing 100 mL SAA solution of different Ct were used to carry out the experimentation, while MFe coupons of 5.0 x 0.08 cm dimensions were suspended with a thread in the solutions. The composition of MFe used in this research was C (2.2-2.9%), Si (0.9-1.9%), Mn (0.15-1.25%), S (0.02-0.2%), P (0.02-0.2%) and the rest Fe. Crude Fe obtained from System Metals Company, Calabar, was pretreated through mirror surface polishing, using 200, 600 and 1200 grit of emery paper. Polished Fe was then washed in distilled water, degreased in ethanol, rinsed in acetone and air dried. The MFe coupons were then stored in an air tight desiccator. The experimentation was set for 60 min interval, after which the coupons were removed, washed in distilled water, degreased and rinsed in ethanol and acetone respectively, then air dried and weighed. The experiment was conducted for 6 h. IE(%) was calculated from Eq. 3.

$$\% J = 100 \text{ x } \left[1 - \frac{r_i}{r_b}\right] \quad (3)$$

where r_b and r_i represent CR of MFe in HCl without and with SAA, respectively.

HER (gasometric) experiment

This experiment was carried out using gasometrical assembly equipment. MFe had dimensions of 2.0 x 0.08 cm. The experimentation was performed following previous works of [15, 18]. IE(%) of SAA was calculated from the CR of MFe from HER volume, according to Eq. 4.

$$Q\% = \frac{\&^0 - \&^i}{\&^0} x\ 100 \quad (4)$$

where $\&^0$ and $\&^i$ are CR of MFe in HCl without and with SAA, respectively, and Q% represents IE(%).

Results

Electrochemical analysis

The calculated values for electrochemical parameters, as displayed in Table 1, were obtained from Fig. 1a, which shows extended positive loops across the different Ct. The highest loop occurred at 7.5 g/L, showing that this Ct of SAA obtained the best inhibition of MFe corrosion in HCl.

$$C_{dl} = \frac{1}{\omega Z''} \quad (5)$$

where Z" is impedance imaginary component, at any frequency inside the semicircle, and ω is angular frequency.

Table 1: Calculated values from Nyquist plots of EIS experiments.

Ct of HCl in M (g/L)	r_{ct} (Ω/cm^{-2})	C_{dl} ($\mu F/cm^{-2}$)	A%
1	97	1.64×10^{-5}	-
1.0	388	4.10×10^{-6}	75.0
2.0	426	3.37×10^{-6}	77.2
3.5	584	2.73×10^{-6}	83.4
5.0	619	2.57×10^{-6}	84.3
7.5	1033	1.54×10^{-6}	90.6

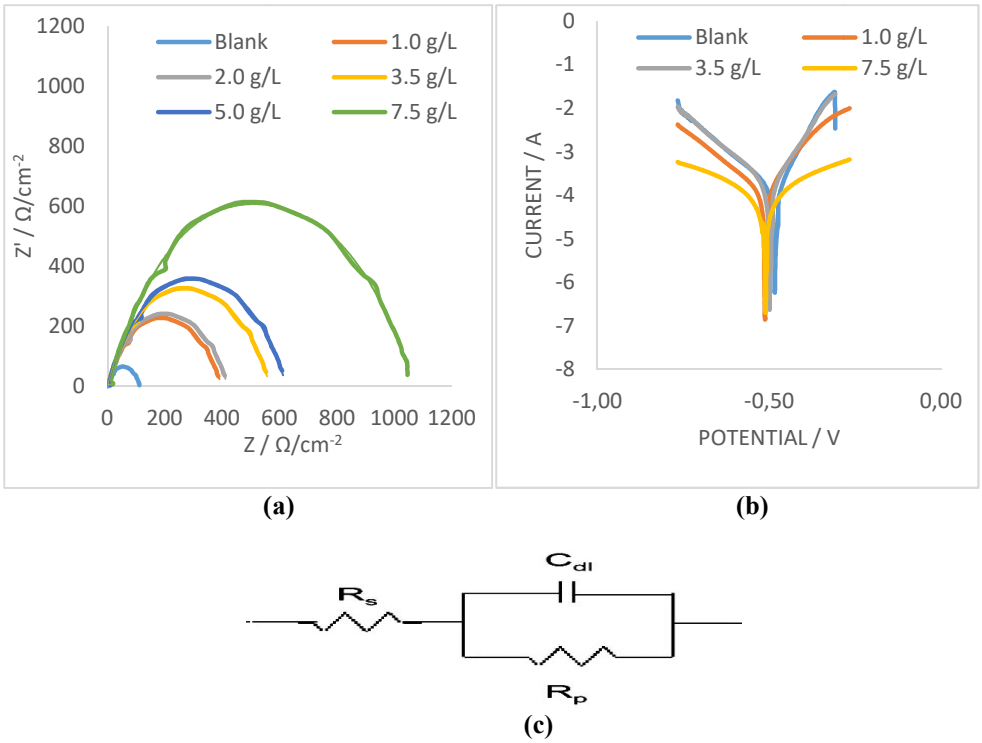

Figure 1: (a) Nyquist plot; **(b)** Tafel plot; and **(c)** electrochemical equivalent circuit diagram for CI of MFe in 1 M HCl.

However, calculated values of IE(%) showed that SAA reduced the trend of MFe anodic dissolution, leading to oxidation, thus protecting the metal from acidic corrosion [16, 19, 20]. This is supported by high R_{ct} values in Table 1, which shows that SAA reduced the possibility of rapid charge transfer across the working electrode (MFe) and HCl, hence protecting it against corrosion [19, 20]. Electrochemical equivalent circuit for EIS is presented in Fig. 1c.
The data for semicircle C_{dl} were determined by Eq. 5, and are shown in Table 1.
I_{corr} aids in explaining the accumulated current charges on the working electrode. This accumulation could enhance or decrease the extent of corrosion effect on the working electrode [17, 18, 21, 22]. Table 2 shows a decrease in I_{corr}, from 6.9 to 0.6 mA/cm^{-2}, for MFe in HCl without and with SAA, respectively, which was derived from Fig. 1b. As I_{corr} values tend to be lower than those of blank HCl, IE(%) values of SAA are expected to be higher at the metal/surface interface. This experience with SAA was typical, as recorded in Table 2, which indicates that it was actively adsorbed onto the working electrode, hence reducing the strong effect of acid corrosion on MFe [10-12]. SAA addition to HCl slightly shifted E_{corr} data, but altered both β_a and β_c values, indicating that it is a mixed type of inhibitor [23].

Table 2: Calculated values from Tafel plots of PDP experiments.

Ct (g/L)	I_{corr} (mA/cm^{-2})	E_{corr} (mV)	β_c (mV/dec)	β_a (mV/dec)	J(%)
Blank	6.911	-806	217	145	-
1.0	1.431	-661	211	110	79.3
3.5	0.519	-652	172	98	92.5
7.5	0.164	-118	109	83	97.6

Computational analysis

It can be seen from Figs. 2a-c that HOMO of SAA is situated at the tropane skeletone, while its LUMO is seen in the benzene ring. HOMO placement in SAA indicates that O and N were the preferential sites for the corrosive attack [13-15].

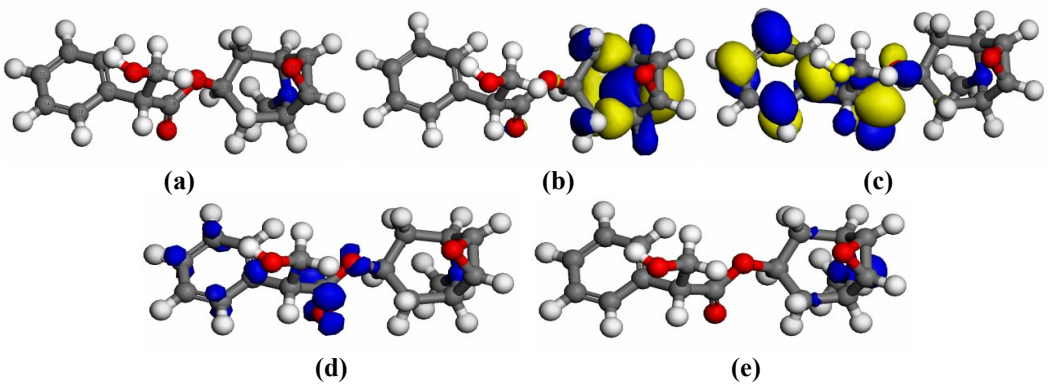

Figure 2: SAA structure showing: **(a)** optimized structure; **(b)** HOMO; **(c)** LUMO; **(d)** adsorption centers for Fukui (+); and **(e)** Fukui (-) functions.

Table 3 presents different quantum values obtained using DFT. Value for change in ΔE was far lower than the threshold, hence explaining better inhibition arising from the possibility of an electron to be removed from HOMO [13]. It is also seen that η value is higher than σ. Literature shows that the more softer a molecule, the more stronger the inhibition trend [14, 15]. Hence, SAA showed an increased IE(%), which was confirmed from μ high value. To affirm the centre of adsorption of the effective constituents adsorbed onto MFe surfaces, Fukui indices were examined on their local reactivity (Figs. 2d and e).

It is clear from Table 3 that N, O, and other C atoms closer to those atoms, could profer perfect adsorption witnessed in the experimental study with alkaloids. SAA has propitious zones for nucleophilic attack located on O_9, O_{11}, O_{12} and N_{20}. SAA has increased dependable sites for its adsorption onto MFe in the HCl solution.

Table 3: Quantum mechanical calculation parameters for SAA major adsorbed compounds.

Parameters	SAA
μ (debye)	1.002
E_{HOMO} (eV)	-3.440
E_{LUMO} (eV)	-1.277
ΔE (eV)	2.163
η	1.510
σ	0.513

WL determination

Slope values from WL plots (mg) *vs*. IT (min) were used to determine CR values, as shown in Table 4. It is seen that WL values of MFe were lower in SAA presence than in its absence. This is always due to SAA molecules strong adsorption onto the MFe exposed corrosion active sites [12, 19, 24].

Table 4: Fukui indices showing local reactivity for SAA.

Negative (-) charge centers	Positive (+) charge centers	Total charges
O_9, O_{11}, O_{12}, C_{14}, C_{19}, N_{20}, C_{21} and C_{22}	C_{10}, C_{13}	10

Since water molecules and O presence around MFe tends to expedite corrosion, it is possible that SAA absence to replace water molecules on the metal created a condition for oxidation at anodic sites. This allowed for corrosion to occur, as seen in CR value for the blank 1 M HCl solution [22-25]. SAA strong adsorption onto the MFe surface led to an increased IE(%) recorded at 98.3%, as shown in Table 5.

Table 5: WL data for CI of MFe by SAA in 1 M HCl.

Ct of HCL in M (g/L)	CR ($mg/cm^2/h$)	SC (θ)	IE(%)
1	7.646	-	-
1.0	4.097	0.464	46.4
2.0	3.267	0.573	57.3
3.5	1.808	0.764	76.4
5.0	1.067	0.860	86.0
7.5	0.127	0.983	98.3

Gasometric analysis

The researchers investigated the effect of different T (313, 323 and 333 K) on SAA, to determine its inhibitive strength. It is seen from Table 6 that SAA showed appreciable inhibition at T up to 333 K. IE(%) was also noticed to increase with higher Ct of SAA, as earlier recorded in WL results. This is applicable to corrosion active sites deactivation by strong adsorption of SAA molecules onto the MFe surface [25, 26]. There was a slight decrease in IE(%) following the rise in T. This is due to SAA molecules gradual desorption caused by strong T and accumulated corrosion particles in HCl [25-27]. However, inhibition was stronger at lower T of 313 K (98.7%), which explains a physical adsorption phenomenon and a possible exothermic reaction, where new bonds are formed between SAA molecules and MFe lattice [28-30].

Table 6: HER data for CI of MFe by SAA in 1 M HCl.

Ct M (g/L)	313 K	323 K	333 K	313 K	323 K	333 K	313 K	323 K	333 K
1 HCl	13.060	17.265	26.809	-	-	-	-	-	-
1.0	4.999	7.989	14.633	0.617	0.537	0.454	61.7	53.7	45.4
2.0	3.066	5.886	10.685	0.765	0.659	0.601	76.5	65.9	60.1
3.5	2.905	3.602	8.682	0.778	0.791	0.676	77.8	79.1	67.6
5.0	0.783	2.167	5.084	0.940	0.875	0.810	94.0	87.5	81.0
7.5	0.175	0.431	2.736	0.987	0.975	0.898	98.7	97.5	89.8

Adsorption mechanism

Langmuir's isotherm was deployed to study SAA nature of adsorption onto the MFe surface, using data generated from gasometric analysis. Table 7 shows various adsorption parameters.

Table 7: Langmuir's isotherm data for MFe CI by SAA in 1 M HCl.

T (K)	Ct (g/L)	R^2	Slope	ΔG^*_{ads} (kJ/mol)
313	0.625	0.9976	1.185	-9.029
323	0.800	0.9922	1.394	-9.966
333	0.839	0.9939	1.575	-10.403

Langmuir's isotherm equation used to calculate the various adsorption parameters is represented in in Eq. 6.

$$\left(\frac{\theta}{1-\theta}\right) = K_{ads}C \qquad (6)$$

where θ and C are SC and Ct of SAA, respectively. A perfect linear R^2 was obtained when data from gasometrical analyses were fitted into Langmuir's isotherm model (Fig. 3), suggesting that SAA adsorption mechanism was consistent with that model [11-13, 31] Eq. 7 was adopted for ΔG_{ads} calculation.

$$K_{ads} = (55.5)^{-1} e^{-\frac{\Delta G_{ads}}{RT}} \qquad (7)$$

where R is universal gas constant (8.314 J/mol^{-1}/K^{-1}) and 55.5 is water Ct in HCl (mol/L^{-1}). Literature reports confirm that K_{ads} high value and ΔG_{ads} low value indicate a strong interaction of SAA with the metal surface and its adsorption onto it [29-32]. Values obtained for those parameters confirmed that SAA showed a strong CI of the MFe surface.

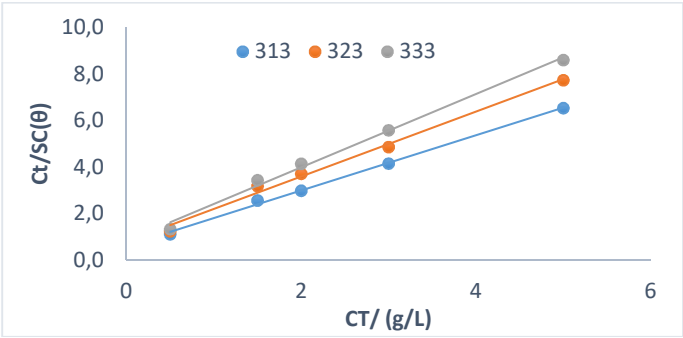

Figure 3: Langmuir's adsorption isotherm diagram for CI of MFe by SAA in a HCl medium.

Thermodynamics investigation

In other to examine the effect of T on the CI action of SAA on the MFe surface, E_a, ΔH_{ads} and ΔS_{ads} were calculated, as shown in Table 8.

Table 8: Thermodynamic data for CI of MFe by SAA in 1 M HCl.

Ct of HCl in M (g/L)	E_a	ΔH_{ads} (kJ/mol)	ΔS_{ads} (kJ/mol)
1	6.9	-8.4	-74.1
1.0	12.0	-15.6	-146.7
2.0	13.1	-16.1	-151.0
3.5	13.3	-16.7	-157.6
5.0	13.7	-18.0	-170.5
7.5	14.5	-21.9	-208.8

These data were derived from Arrhenius and transition state equation plots in Figs. 4a and b. From Table 8, it was confirmed that E_a data obtained for MFe with SAA were higher than those without it, and lower than 20 kJ/mol^{-1}. This indicates that SAA adsorption was best at lower T, and that it was physical, which confirms results from gasometrical analyses [30, 33]. It also reveals that the system was required to overcome more energy for the corrosion reaction to occur, due to SAA molecules stronger adsorption onto the MFe surface. The analyses also revealed negative ΔH_{ads} and values lower than 80 kJ/mol^{-1}, which indicates an exothermic reaction where new bonds were formed between SAA molecules and MFe lattice. SAA was also physically adsorbed, which confirms results from gasometrical analysis [22-23, 34]. The reaction was stable and spontaneous in the forward direction, and with a significantly lesser degree of disorderliness, as shown by ΔG_{ads} (< 20 kJ/mol) and ΔS_{ads} values [16-19, 34-35].

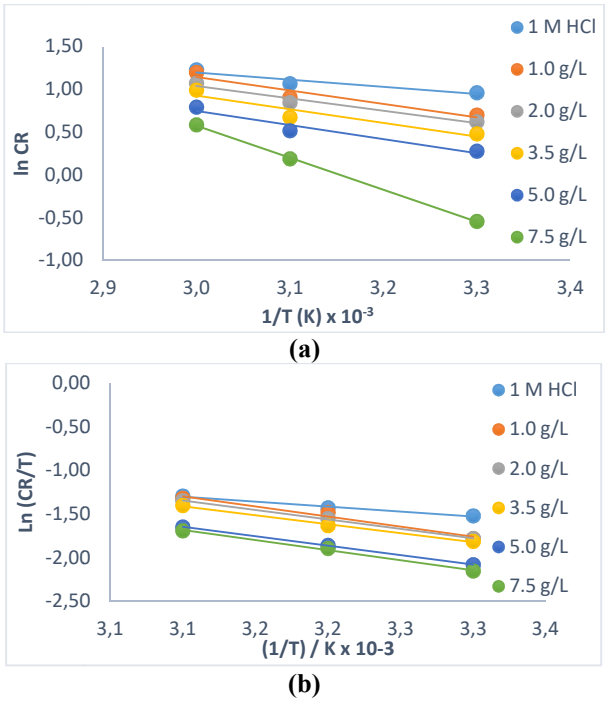

Figure 4: (a) Arrhenius and **(b)** transition state plots for CI of MFe by SAA in HCl.

SEM analysis

Figs. 5 a-c show images obtained for the working electrode (MFe) scanning in HCl without SAA and with its Ct of 1.0 and 7.5 g /L, respectively.

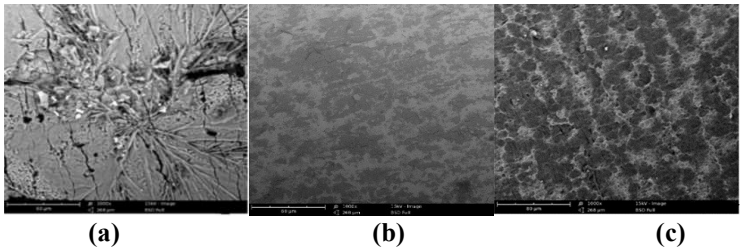

(a) **(b)** **(c)**

Figure 5: Images obtained from SEM for Fe corrosion in: **(a)** pure 1 M HCL; **(b)** with 1.0 g/L SAA; and **(c)** with 7.5 g/L SAA.

Fig. 5a depicts strong and aggressive attack from HCl on MFe, due to corrosion effects [32-34]. However, SAA addition, at 1.0 g/L Ct, caused an appreciable decrease in metal surface roughness. Complete smoothness was achieved with a higher Ct of SAA (7.5 g/L). This could be due to large SC of the MFe surface by SAA, which protected both anodic and cathodic active sites from corrosion activation [10, 32-34].

Conclusion

It was observed from the various experiments that SAA perfectly mitigated MFe corrosion, with IE(%) up to 90.6, 97.6, 98.3 and 98.7%, for EIS, PDP, WL and HER results, respectively. SAA showed significant stability and less disorderliness while in contact with the MFe surface, through a physical adsorption phenomenon. SAA increased the reaction E_a, leading to higher energy requirement for corrosion to occur between it and MFe. Theoretical data show that SAA created a shorter ΔE between different bands of MFe, which allowed for an easy transition of the inhibitor molecules, hence establishing a speedy and stronger adsorption. All results obtained from in the experimental analyses in the study agreed.

Competing interest

The authors declare that there is no conflict of interest in the research work.

Authors' contributions

B. U. Ugi: research design; data analysis and interpretation of results; manuscript writing. **J. E. Boekom**: data analysis; manuscript proofreading. **P. B. Ashishie**: material collection; laboratory work; manuscript review. **P. U. Ubua**: laboratory experimentation; manuscript proofreading.

Abbreviations

C_{dl}: double layer capacitance
CI: corrosion inhibitors
CR: corrosion rate
Ct: concentration
DFT: density functional theory
E_a: activation energy
E_{corr}: corrosion potential
E_{HOMO}: energy of the highest occupied molecular orbital
EIS: electrochemical impedance spectroscopy
E_{LUMO}: energy of the lowest occupied molecular orbital
HCl: hydrochloric acid
HER: hydrogen evolution reaction
HOMO: highest occupied molecular orbital
I_{corr}: corrosion current
IE(%): inhibition efficiency
IT: immersion time
J: current density

K_{ads}: equilibrium constant of the adsorption–desorption
LUMO: lowest unoccupied molecular orbital
MFe: malleable Fe
PDP: potentiodynamic polarization
R^2: regression coefficient
R_{ct}: charge transfer resistance
SAA: scopolamine alkaloid
SC: surface coverage (θ)
SCE: saturated calomel electrode
SEM: scanning electron microscopy
T: temperature
WL: weight loss

Symbols definition

β_a: anodic Tafel slope
β_c: cathodic Tafel slope
ΔE: energy gap
ΔH_{ads}: standard enthalpy of adsorption
$\Delta G°_{ads}$: standard free energy of adsorption
ΔS_{ads}: standard entropy of adsorption
η: global hardness
μ: dipole moment
π: chemical potential
σ: global softness

References

1. Fajobi MA, Fayomi OSI, Akande IG et al. Inhibitive Performance of Ibuprofen Drug on Mild Steel in 0.5 M of H_2SO_4 Acid. J Bio-Tribo Corr. 2019;5:1-5. http://doi.org./10.1007/s40735-019-0271-3
2. Fouda AES, El-Askalany AH, Molouk AFH et al. Experimental and computational chemical studies on the corrosion inhibitive properties of carbonitrile compounds for carbon steel in aqueous solution. Sci Reps. 2022;11:67- 79. http://doi.org./10.1038/s41598-021-00701-z
3. Kadhim A, Betti N, Al-Adili A et al. Limits and developments in organic inhibitors for corrosion of mild steel: a critical review (Part two: 4-aminoantipyrine. Int J Corr Scale Inhib. 2022;11:46-63. http://doi.org./10.17675/2305-6894-2022-11-1-2
4. Bashir S, Sharma V, Kumar S et al. Inhibition performances of Nicotinamide against aluminum corrosion in an acidic medium. Port Electrochim Acta. 2020;38,107-123. http://doi.org./10.4152/pea.202002107
5. Bhuvaneswari R, Santhakumari C, Usha et al. Synthesis, growth, structural, Spectroscopic, optical, Thermal, DFT, HOMO–LUMO, MEP, NBO analysis, and thermodynamic properties of vanillin isonicotinic hydrazide single crystal. J Mol Struc. 2021;4:130856. http://doi.org./10.1016/j.molstruc.2021.130856

6. Bilgic S. Plant extracts as corrosion inhibitors of mild steel in H_2SO_4 and H_3PO_4 media- Review II. Int J Corr Scale Inhib. 2022;11:1-42. http://doi.org./10.17675/2305-6894-2022-11-1-41
7. Boumhara K, Harhar H, Tabyaoui M et al. Corrosion inhibition of mild steel in 0.5 M H_2SO_4 solution by *Artemisia herba-alba* Oil. J Bio-Tribo Corr. 2019;5:1-8. http://doi.org./10.1007/s40735-018-0202-8
8. Dagdag O, El Harfi A, Cherkaoui O et al. Rheological, electrochemical, surface, DFT and molecular dynamics simulation studies on the anticorrosive properties of new epoxy monomer compound for steel in 1 M HCl solution. RSC Adv. 2019;9:4454-4462. http://doi.org./10.1039/c8ra09446b
9. Diki NYS, Coulibaly NH, Kambire O et al. Experimental and theoretical investigations on copper corrosion inhibition by cefixime drug in 1 M HNO_3 solution. J Mater Sci Chem Eng. 2021;9:11-28. http://doi.org./10.4236/msce.2021.95002
10. Doubi M, Erramli H, Touir H et al. A synthesis 3-phenyl-1, 2, 4-triazole-5-thione as an inhibitor against low carbon steel corrosion in simulated reinforced concrete: experimental and theoretical studies. Chem Data Collec. 2023;44:100989. https://doi.org/10.1016/j.cdc.2023.100989
11. Gadow HS, Fakeeh M. Green inhibition of carbon steel corrosion in 1 M hydrochloric acid: *Eruca Sativa* seed extract (experimental and theoretical studies). RSC Adv. 2022;12:8953-8986. http://doi.org./10.1039/D2RA01296K
12. Ahmed AF, Hossam EA, Emad AB et al. The inhibition performance of morpholinium derivatives on corrosion behavior of carbon steel in the acidized formation water: Theoretical, experimental and biocidal evaluations. J Mol Liqs. 2021;341:117348. https://doi.org/10.1016/j.molliq.2021.117348
13. Agwamba EC, Udoikono AD, Hitler L et al. Synthesis, characterization, DFT studies and molecular modeling of azo dye derivatives as potential candidate for trypanosomiasis treatment. Chem Phys Imp. 2022;4:100076. http://doi.org./10.1016/chphi.2022.100076
14. Ammouchi N, Allal H, Belhocine Y et al. DFT computations and molecular dynamics investigations on conformers of some pyrazinamide derivatives as corrosion inhibitors for aluminum. J Mol Liqs. 2020;300:112309. http://doi.org./10.1016/j.molliq.2019.112309
15. Hashem HE, Farag AA, Eslam M et al. Experimental and theoretical assessment of benzopyran compounds as inhibitors to steel corrosion in aggressive acid solution. J Mol Struct. 2021;1249:131641. https://doi.org/10.1016/j.molstruc.2021.131641
16. Iroha NB, Nnanna LA, Maduelosi NJ et al. Evaluation of the anticorrosion performance of *Tamsulosin* as corrosion inhibitor for pipeline steel in acidic environment: experimental and theoretical study. J Taibah Univ Sci. 2022;16(1):288-299. https://doi.org/10.1080/16583655.2022.2048512
17. Joycee SC, Raja AS, Rajendran S et al. Corrosion mitigation by an eco-friendly inhibitor: *Beta vulgaris* (beetroot) extract on mild steel in simulated oil well water medium. Int J Corr Scale Inhib. 2022;11:82-101. http://doi.org./10.17675/2305-6894-2022-11-1-4

18. Laadam G, El Faydy M, Benhiba F et al. Outstanding anti-corrosion performance of two pyrazole derivatives on carbon steel in acidic medium: Experimental and quantum-chemical examinations. J Mol Liqs. 2023;2:121268. https://doi.org/10.1016/j.molliq.2023.121268
19. Ugi BU, Obeten ME, Bassey VM et al. Adsorption and inhibition analysis of aconitine and tubocurarine alkaloids as eco-friendly inhibitors of pitting corrosion in ASTM – A47 low carbon steel in HCl acid environment. Indones J Chem. 2022;22:1- 16. http://doi.org./10.22146/ijc.56745
20. Liu Q, Song Z, Han H et al. A novel green reinforcement corrosion inhibitor extracted from waste *Platanus acerifolia* leaves. Constr Build Mater. 2020;260:119695. http://doi.org./10.1016/j.conbuildmat.2020.119695
21. Majda MT, Ramezanzadeh M, Ramezanzadeh B et al. Production of an environmentally stable anti-corrosion film based on *Esfand* seed extract molecules- metal cations: Integrated experimental and computer modeling approaches. J Hazard Mater. 2020;382:1-16. http://doi.org./10.1016/j.hazmat.20192019.121029
22. Ugi BU, Obeten M. Inhibition of limestone ($CaCO_3$) concentrated rich water effects on zinc sheets using crude alkaloids and non alkaloids extracts of *Nepeta cataria* (Catnip) plant. Int J Innov Sci Engr Tech. 2019;6(3):74-81.
23. Onyeachu IB, Abdel-Azeim S, Chauhan DS et al. Electrochemical and Computational insights on the application of expired Metformin drug as a novel inhibitor for the sweet corrosion of C1018 steel. ACS Omega. 2021;6:65-76. http://doi.org./10.1021/acsomega.0c03364
24. Parajuli D, Sharma S, Oli HB et al. Comparative study of corrosion inhibition efficacy of alkaloid extracts of *Artemesia vulgaris* and *Solanum tuberosum* in mild steel samples in 1 M sulphuric acid. Electrochemistry. 2022;3:416-433. http://doi.org./10.3390/electrochem3030029
25. Rbaa M, Ouakki M, Galai M et al. Simple preparation and characterization of novel 8-Hydroxyquinoline derivatives as effective acid corrosion inhibitor for mild steel: Experimental and theoretical studies. Coll Surf A: Physicochem Eng Asps. 2020;602:125094. http://doi.org./10.1016/j.colsurfa.2020.125094
26. Sharma S, Ganjoo R, Saha SK et al. Experimental and theoretical analysis of baclofen as a potential corrosion inhibitor for mild steel surface in HCl medium. J Adhes Sci Tech. 2021;1:19-32. https://doi.org/10.1080/01694243.2021.200230
27. Tsygankova LE, Uryadnikov AA, Abramov AE et al. Inhibiting formulations against hydrogen sulfide corrosion of carbon steel. Int J Corr Scale Inhib. 2022;11:102-110. http://doi.org./10.17675/2305-6894-2021-11-1-45
28. Ugi BU. Corrosion Inhibition of Cu-Zn-Fe Alloy in hydrochloric acid medium by crude ethanol extracts from roots-leaves synergy of *Solanum melongena*. Earthline J Chem Sci. 2021;5(1):105-118.
29. Ebenso EE, Verma C, Olasunkanmi LO et al. Molecular modelling of compounds used for corrosion inhibition studies: a review. Phys Chem Chem Phys. 2021;23:19987-20027. http://doi.org./10.1039/D1CP00244A

30. Erteeb MA, Ali-Shattle EE, Khalil SM et al. Computational studies (DFT) and PM3 theories on thiophene oligomers as corrosion inhibitors for iron. Amer J Chem. 2021;11:1-7. http://doi.org./10.5923/j.chemistry.20211101.01
31. Ugi BU, Obeten ME, Bassey VM et al. Quantum and electrochemical studies of corrosion inhibition impact on industrial structural steel (E410) by expired amiloride drug in 0.5 M solutions of HCl, H_2SO_4 and $NaHCO_3$. Mor J Chem. 2021;9(4):677-696. https://doi.org/10.48317/IMIST.PRSM/morjchem-v9i3.22346
32. Iroha NB, Maduelosi NJ, Nnanna LA et al. The impact of tizanidine on E24 carbon steel corrosion inhibition in oilfield acidizing solution: experimental and quantum chemical studies. Emerg Mater. 2022;1:111-121. https://doi.org/10.1007/s42247-022-00400-z
33. James AO, Iroha NB. New green inhibitor of *Olax subscorpioidea* root for J55 carbon steel corrosion in 15% HCl: theoretical, electrochemical, and surface morphological investigation. Emerg Mater. 2022;5:1119-1131. https://doi.org/10.1007/s42247-021-00161-1
34. Joshi BD, Thakur G, Chaudhary MK et al. Molecular structure, homo-lumo and vibrational analysis of ergoline by density functional theory. Sci World. 2021;14:21-30. http://doi.org./10.3126/sw.v14i14.34978
35. Uwah IE, Ugi BU, Okafor PC et al. Investigation of the corrosion inhibition effects of bitters on mild steel in acidic medium: A case study of *Andrographis paniculata* and *Vernonia amygdalina*. Proceed 35th Int Conf Chem Soc Nig. 2012;2:304-309.